

*Chapter 5*LINEAR DYNAMICS IN NONLINEAR LATTICES: LOCAL TO EXTENDED
TRANSITIONS OF RESONANT DEFECT MODES

We study the localized modes created by introducing a resonant defect in a mechanical lattice. We find that modes introduced by resonant defects have profiles that can be tuned from being extremely localized to totally delocalized by an external force. This is in direct contrast with modes introduced by traditional mass or stiffness defects, in which the modes' profiles stay constant. We present an analytical model for resonant defects in one-dimensional nonlinear lattices, computationally demonstrate the equivalent effect in a two-dimensional lattice, and experimentally observe the mode profiles in a granular crystal. While our study is concerned with nonlinear mechanical lattices, the generality of our model suggests that the same effect should be present in other types of periodic lattices.

5.1 Introduction

The ability to actively control a material's properties through external stimuli is rare and is a goal of materials design^{16,101}. Defects have an enormous effect on material properties: electrical conductivity in semiconductors¹², thermal conductivity¹³, and mechanical strength^{14,15} are just a few examples. This is in part because defects in periodic lattices allow for local modes of vibration that interact with propagating waves and affect material properties⁴⁴⁻⁴⁷.

The periodicity of crystals lattices may result in frequency bands and band gaps¹⁰. Modes that are in the frequency band extend the entire length of the crystal. In contrast, a mode with

frequency in the band gap is not extended but spatially localized. A defect breaks the symmetry of the lattice and can introduce such a localized mode. The mode's spatial extension depends on where its frequency lies in the band gap. As the mode's frequency gets closer to a band, the mode profile becomes more delocalized. In traditional mass or stiffness defects, external effects that shift the band frequencies also introduce a proportional shift in the defect mode frequency, rendering the profile of the defect mode insensitive to external influences. This means that for most defects, the localization is determined by the defect to lattice mass ratio²⁷. We show that for a resonant defect the prescribed relationship between mode frequency and band frequency does not exist, and hence the mode profile can be tuned by an external force. This is due to an additional degree of freedom provided by the displacement of the secondary mass⁴⁸. Control over the localization is interesting to applications of defect modes^{50,102-104}, since many properties, for example the wave speed in coupled resonant optical waveguides^{50,105} and the coupling of phonon-photon interactions¹⁰², depend on the spatial overlap of modes.

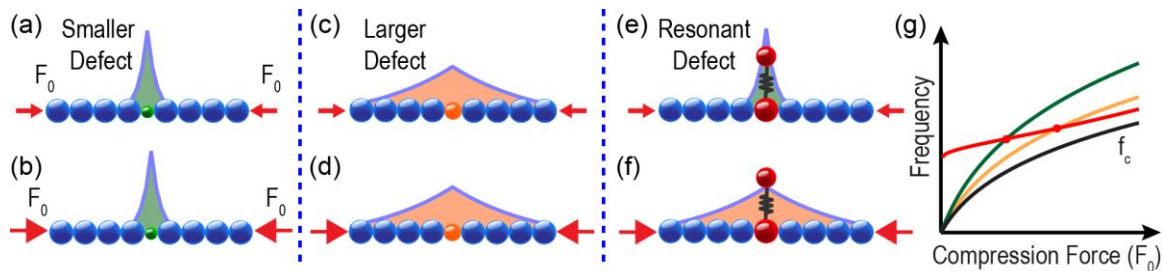


Figure 5.1: A schematic illustrating defect induced local modes and resonant defect tunability. (a),(c), and (e), represent the lattice subject to lower compression, while (b),(d), and (f) represent a higher compression. (a) and (b) show a mode due to a small defect (green) that is highly localized and does not change its profile between low (a) and high compression (b). (c) and (d) show that the mode due to a larger (red) defect is less localized and still does not depend on compression. (e) and (f) show a mode created by a resonant defect (red) in which the localization can be tuned to from highly localized to completely delocalized. (g) illustrates the origin of this tunability. The small (green) and large (orange) defect frequencies maintain a

constant proportion with the band cutoff frequency, resulting in an unchanged localization. In the case of the resonant defect (red) frequency, this constant proportionality is not prescribed. Thus, compression changes the spatial profile of a resonant defect mode.

5.2 Tuning mode profiles

We study the dynamics of a local mode and observe how it transitions from highly localized to completely delocalized as a result of an external compression. Figure 5.2 shows the steady state force measured in the particle next to the resonant defect (Fig. 5.2a) and at the end of the chain (Fig. 5.2b). This dynamic force results from a harmonic excitation at the defect's resonating mass. The measured force is a function of the excitation frequency and static compression. On top of the experimental results, the theoretical expression for the band edge in a granular crystal is plotted as a white dotted line, $f_c = 4.9 \cdot F_0^{1/6}$ [kHz]. Below this line, we see the individual modes of the band rise up in frequency as the compression increases. Since the force sensor in Fig. 5.2a is next to the defect, this measures both local and extended dynamic forces. Figure 5.2a shows the presence of the defect resonance mode (varying slightly around 6.2 kHz) at all compressions. This defect mode frequency increases only a few Hz as a result of increasing compression. This is due to the small mass participation, m_r , of the resonating structure. Figure 5.2b shows the force in the sensor at the end of the chain. This sensor measures only the extended modes, i.e., effects far away from the defect. This sensor does not detect the defect mode until the band edge crosses the mode's frequency at approximately 4 N. Beyond this compression, the defect mode becomes extended and the excitation propagates through the crystal. This shows that a single resonant defect can be tuned to an arbitrary effective size.

More insight on the defect mode's dependence on compression can be seen in Fig. 5.2c, 5.2d, and 5.2e, which show the mode's spatial profile at three increasing compressions, corresponding to the dashed vertical dashed lines in Fig. 5.2a and 5.2b. The left two panels (Fig. 5.2c and 5.2d) are measured at compressions while the mode is still localized, before the dynamics are extended. As the granular crystal is compressed and the acoustic band edge approaches the mode and the mode begins to delocalize, i.e., the exponential attenuation decreases. Above a certain compression the acoustic band rises above the defect mode frequency and the dynamics transition to extended. An analogous tuning and transition has been achieved by geometrically altering defect cavity layers in phononic superlattices¹⁰⁴. The rightmost panel (Fig. 5.2e) shows the extended mode profile at a higher compression. This reveals why there is little force observed in Fig. 5.2b until high compressions.

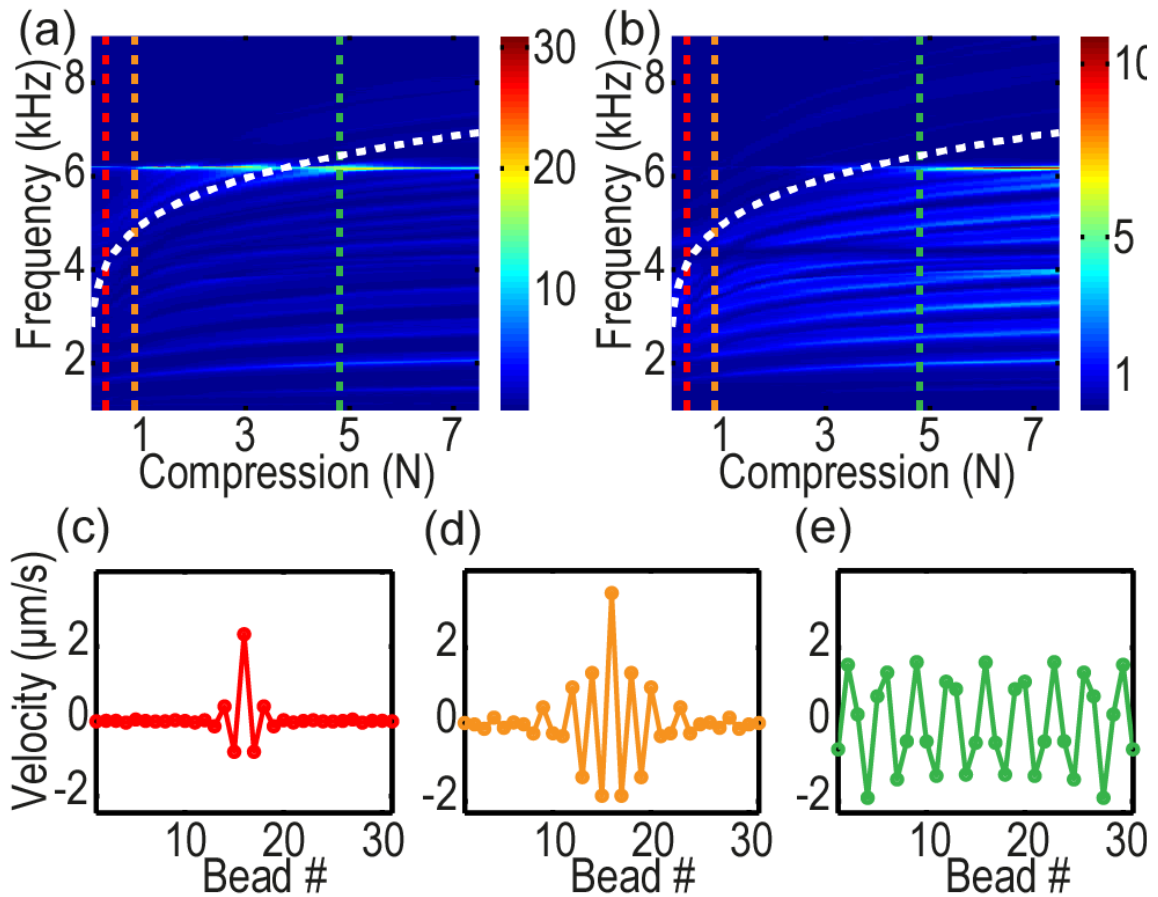


Figure 5.2: The acoustic band and defect mode profile evolution. The color scale shows the steady state amplitude at the embedded force sensors as a function of the frequency and the static compression (a) next to the defect and (b) at the crystal's edge. The defect mode, around 6.2 kHz, appears in the force sensor at the crystal's edge only after the band edge rises above the frequency of the defect mode (at 4 N). The mode's frequency increases very slightly as the lattice is compressed. The dotted curve is the theoretical edge of the acoustic band. (c),(d), and (e) show the local mode profile measured at three different compressions (0.3 N, 0.9 N, and 4.8 N), which are indicated as dotted vertical lines in (a) and (b). At higher compressions, shown in (e), the mode transitions to being completely extended and the dynamics are delocalized. The measurements are performed for half of the chain and we plot their mirrored image of the other half for clarity.

The underlying physics of the problem can be understood through an analytical model for a resonant defect between two semi-infinite generic lattices (see Section 5.4). We quantify the mode's spatial localization using an exponential decay factor, L , defined as the ratio of the

displacement amplitude between neighboring particles. This localization depends explicitly on the ratio, f_c/f_d , of the band edge cutoff to the defect mode's frequencies,

$$L = \frac{2f_d^2}{f_c^2} \left[1 \pm \sqrt{1 - \frac{f_c^2}{f_d^2}} \right] - 1. \quad (5.1)$$

Therefore, a resonant defect mode's localization can be controlled by changing this ratio, which is accomplished through an external compression. However, since the defect mode is actually a mode of the entire lattice, the defect mode frequency also depends on the compression, or equivalently on the band edge, $f_c \propto F_0^{1/6}$. The defect mode frequency can be found solving the implicit equation,

$$\frac{m_r}{m_0} = \left(1 - \frac{f_d^2}{f_r^2} \right) \left[\frac{m_s}{m_0} \left(1 \pm \sqrt{1 - \frac{f_c^2}{f_d^2}} \right) - 1 \right]. \quad (5.2)$$

Together these two equations describe the defect mode localization's dependence on compression, or equivalently on the acoustic band edge.

Figure 5.3a shows a comparison between the analytical solution in an infinite lattice with computational results for solving the eigenvalue problem for a finite chain of 31 particles. We can see that the boundary effects play a negligible role until just before the mode theoretically delocalizes. Figure 5.3a shows three horizontal dashed lines, corresponding to the localization calculated for three different simple mass defect diameters, 11.1 mm, 14.3 mm, and 17.5 mm. The smallest defect results in the greatest localization. This demonstrates that by changing the

external compression, the resonant defect mode localization is similar to that of mass defects of differing sizes.

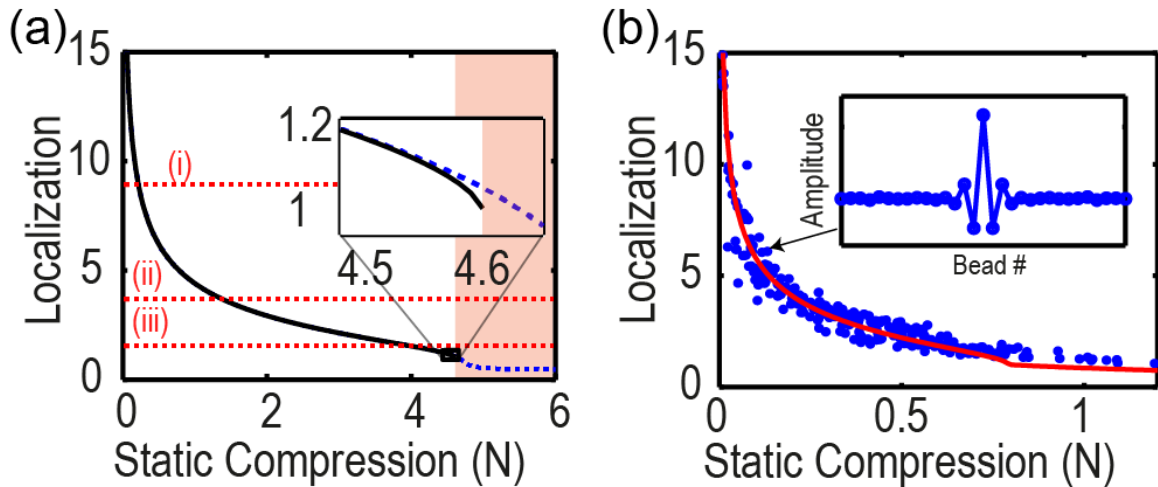


Figure 5.3: Tunable Localization of a resonant defect mode. (a) Localization factor predicted analytically (solid line) for an infinite lattice and calculated computationally for a 31 particle chain (dashed line). Three horizontal dashed lines (i), (ii), and (iii) show localizations for different defect diameters, 11.1 mm, 14.3 mm and 17.5 mm, respectively. In addition, all parameters used in the computation are the derived from the experimental setup. The inset in (a) is an enlarged view, showing the deviation of the computational and analytical results close to the when the defect frequency and band edge meet. (b) The experimentally measured localization and a fit (red line) to the analytical prediction. Each experimental run is shifted along the compression axis to have the same zero point. The inset shows the mode profile used to measure the experimental localization for the run indicated by the arrow.

The experimental measurements of the localization factor as a function of different compressions are shown in Fig. 5.3b, for over 26 independent tests. We fit these experimental results to our analytical model (Eq. 5.2). The analytical model accurately captures the localization's dependence on compression. We attribute the disagreement between the theoretical (Fig. 5.3a) and experimental (Fig. 5.3b) compression scale to friction effects, originating from the large mass of the resonator and significant contact area between the particles and supporting rods.

We computationally study resonant defect modes in a two-dimensional hexagonal lattice with nearest neighbor interactions. Although, the dynamics become more complex due to the presence of both transverse and longitudinal acoustic modes of the crystal, the defect modes' profiles can still be tuned through an external pressure. To understand the dynamics without a defect present, we first found the longitudinal and transverse branches applying periodic Bloch conditions (see section 5.3) and solving the eigenvalue problem. Then we include the defect mode, and confirm that as the defect mode frequency passes below the upper edge of the longitudinal acoustic band, the mode delocalizes, similar to the case of the one-dimensional granular crystal. Figure 5.4 illustrates the mode profile of a resonant defect in a finite lattice at two different isotropic compressions.

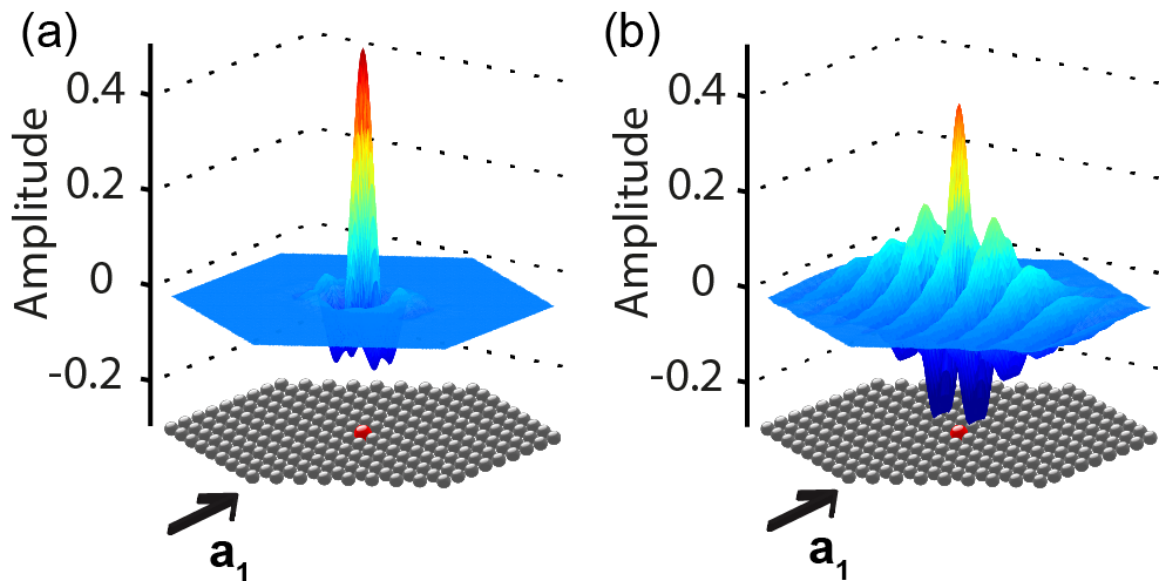


Figure 5.4: Resonant Defects in Hexagonal Lattices. The normalized mode profile due to a resonant defect (red) placed in a two dimensional hexagonal lattice (grey). We plot the amplitude of the particles displacement in the nearest neighbor direction, \mathbf{a}_1 . The mode becomes less localized as it goes from low (a) to high (b) isotropic compression.

5.3 Applications of tuning mode profiles

Ultraslow wave propagation

Coupled resonant optical waveguides use tunneling between strategically placed defects to enable the optical transmission of information. The placement and separation between the defects is used to control the speed of wave propagation[16]. Using this as inspiration, we can flip this idea and control the effective separation by dynamically changing the mode's localization. When a defect mode is highly localized the periodically placed resonant defects are effectively further apart. For weakly localized defect modes, the modes overlap more, and are effectively closer together. Therefore, controlling the localization of the modes also affects their coupling, and the wave speed can be dynamically tuned.

We have demonstrated this concept numerically by solving the system shown in Fig. 5.5a when subjected to periodic Bloch wave conditions. The periodicity of the system leads to a narrow band region in which the wave energy is primarily located in the resonant masses. This bandwidth is an effective measure of the average group velocity for a wave packet located at this frequency and can be tuned to achieve ultraslow acoustic wave propagation in materials. Fig. 5.5b illustrates the extent of the dynamic control and the potential for ultraslow velocity propagation.

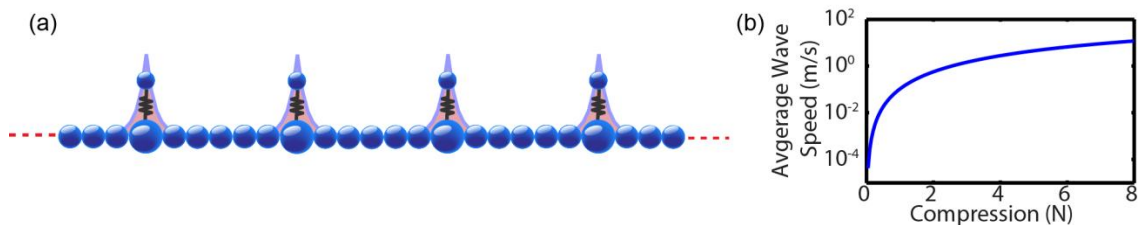


Figure 5.5: Ultraslow velocity wave propagation. (a) A design proposal for achieving tunable ultraslow acoustic or phononic propagation. (b) The wave velocity of the

high frequency narrow band waves in the schematic shown in (a). These results were numerically calculated by applying Bloch conditions to the six particle unit cell.

Tunable scattering relaxation times

Thermal conductivity depends strongly on phonon scattering mechanisms of a crystal. These scattering phenomena can be quantified by the relaxation time constant, τ , which is a result of a variety of effects: Rayleigh scattering from mass or density fluctuations in a crystal, Umklapp scattering between phonons, boundary effects, and resonance scattering from localized modes. The time constants from each effect contribute to the total time constant as a sum of reciprocals,

$$\tau^{-1} = \sum_i \tau_i^{-1}. \quad (5.3)$$

Pohl et al. and Wagner demonstrated that a type of resonance scattering due to localized modes in a crystal makes a significant contribution [7,35]. In the model two phonons collide and are temporarily trapped in an excited state of the localized mode. The scattering relaxation time of this effect is directly dependent on the exponential localization of the mode. We show that this can be localized and controlled through an external stimulus, therefore also giving control over phonon scattering.

2D numerical analysis

We examine the tunability of local defect modes in a hexagonal lattice in two dimensions with nearest neighbor coupling. For a two dimensional system, the coupling stiffness can also be tuned through compression. By applying periodic Bloch conditions, we find the band structure for the monoatomic lattice dynamics (Fig. 5.6). In order to study a tunable defect in this

lattice, we construct a model for an isotropic resonant defect placed at the center of a finite crystal. Since the host lattice has a transverse and longitudinal phonon branch, introducing a defect results in two additional modes, one for each degree of freedom. The two modes delocalize at different compressions.

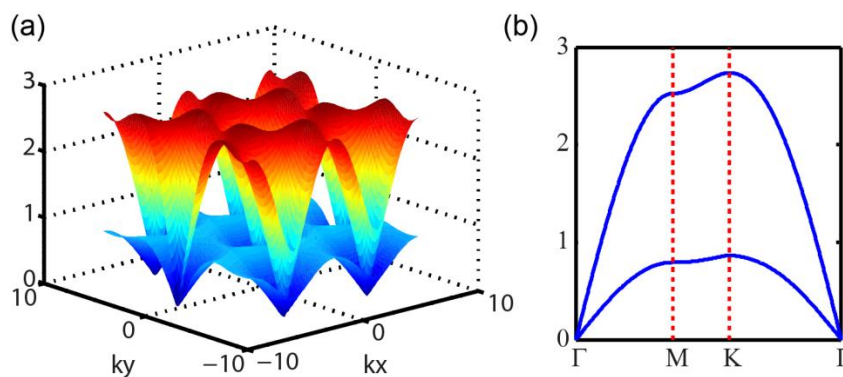


Figure 5.6: Phonon Band Structure for a two dimensional hexagonal lattice . (a) The 2-D band surface with associated cuts (b) along high symmetry directions of a hexagonal lattice. This figure illustrates the acoustic transverse and longitudinal phonon bands.

5.4 Analysis

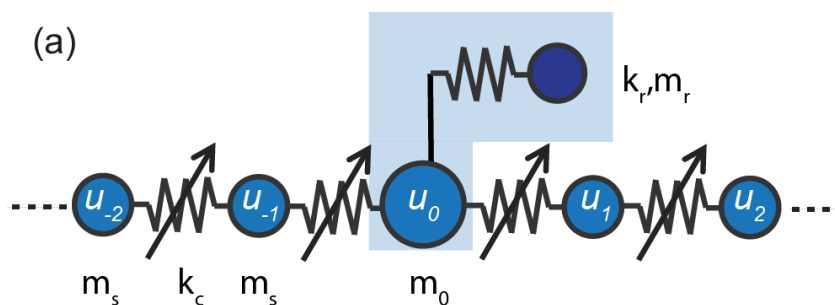


Figure 5.7: Analytical model. (a) A schematic for the analytical model including relevant parameters.

We start by combining the solution for an infinite chain[11] with the frequency dependent effective mass[13] of a resonator particle (Fig. 5.7). If we consider a solution above the

acoustic band of the crystal then the known solution is oscillatory and exponentially localized. This means that the amplitude decays exponentially in both directions by a localization factor L ,

$$u_{-i} = u_{+i} = \frac{u_0}{(-L)^i}. \quad (5.4)$$

In 1-D linear lattices solutions for the j^{th} particle in the equations of motion are described by $u_j = e^{i(kj - \omega t)}$. When the wavenumber is real the solution is extended. However, when the frequency is above the acoustic band edge, the wavenumber has a nonzero imaginary component, and the solution decays. The localization factor that we present is the ratio of amplitudes and is related to the wave number as, $L = -e^{\pm ik}$. When the wavenumber is complex the localization is real.

By considering the solution in one of the semi-infinite lattices, at either side of the defect, $i \neq 0$, we can find how this localization factor depends on frequency. The equation of motion is,

$$-m_s \omega^2 u_i = k_c (u_{i+1} + u_{i-1} - 2u_i). \quad (5.5)$$

By both assuming an oscillatory solution at frequency ω and using the above relation, the equation for particle i 's displacement, u_i , becomes a quadratic equation for L ,

$$L^2 + (2 - 4\omega^2/\omega_c^2)L + 1 = 0, \quad (5.6)$$

where $\omega_c = 2\sqrt{k_c/m_s}$ is the frequency of the acoustic band edge. The solution to (Eq. 5.6) gives the localization factor, L ,

$$L = \frac{2\omega^2}{\omega_c^2} \left[1 \pm \sqrt{1 - \frac{\omega_c^2}{\omega^2}} \right] - 1. \quad (5.7)$$

The equation for L has two solutions where $L_+ = 1/L_-$. This reflects the perspective of the exponential attenuation. In one direction the amplitude is decaying and divided by the factor L , while in the other direction the amplitude is increasing and is multiplied by L . The equation illustrates that the defect mode localization only depends on the ratio of the defect mode frequency to the band edge frequency.

Now we consider an infinite lattice with a single defect at site $i = 0$. The system can be described by the set of equations:

$$-\omega^2 m_i u_i = k_c (u_{i-1} + u_{i+1} - 2u_i), \quad (5.8)$$

where $m_i = m_s$ for all $i \neq 0$. The defect has a frequency dependent effective mass, $m_{eff} = m_0 \left[1 + \frac{m_r}{m_0} \left(1 - \frac{\omega^2}{\omega_r^2} \right)^{-1} \right]$. This replaces the two masses, m_r and m_0 , and spring constant, k_r , describing the defect with $\omega_r = \sqrt{\frac{k_r}{m_r}}$. With a little algebraic manipulation, and again, assuming an oscillatory and exponentially decaying solution supp. (1) , the equation of motion (Eq. 5.8) for the defect particle becomes,

$$m_{eff}\omega^2 = 2k_c \left(\frac{1}{L} + 1 \right). \quad (5.9)$$

Now we can easily plug in for the localization, L , and effective mass, m_{eff} , to arrive at the analytical expression comparing mass ratio and frequencies:

$$\omega^2 m_0 \left(1 + \frac{\frac{m_r}{m_0}}{\left(1 - \frac{\omega^2}{\omega_r^2}\right)} \right) = 2k_c \left(\frac{2\omega^2}{\omega_c^2} \left[1 \pm \sqrt{1 - \frac{\omega_c^2}{\omega^2}} \right] \right). \quad (5.10)$$

By plugging the equation for the direction of L_+ and changing angular frequencies to real frequencies we arrive at the following equation:

$$\frac{m_r}{m_0} = \left(1 - \frac{f_d^2}{f_r^2} \right) \left[\frac{m_s}{m_0} \left(1 \pm \sqrt{1 - \frac{f_c^2}{f_d^2}} \right) - 1 \right]. \quad (5.11)$$

The masses, m_r , m_0 , and characteristic frequency, f_r , of the resonant defect depend on geometry and material, and are therefore a design consideration and do not lead to any dynamics control. In the granular crystal the cutoff frequency depends on static compression

$$f_c = \frac{1}{2\pi} \sqrt{\frac{6}{m_s}} A^{1/3} F_0^{1/6}.$$

Comparison with simple mass defect

Now we can compare this expression with that derived for a mass defect. The equation describing a mass defect can be derived in the same way, except the mass is not an effective mass but instead m_0 .

$$\frac{m_0}{m_s} = \left[1 \pm \sqrt{1 - \frac{\omega_c^2}{\omega^2}} \right]. \quad (5.12)$$

This equation can easily be solved for the frequency of the mode.

$$\frac{\omega^2}{\omega_c^2} = \left[1 - \left(\frac{m_0}{m_s} - 1 \right)^2 \right]^{-1}. \quad (5.13)$$

It is clear from this equation, that the frequency of the mode (and therefore the localization) depends only on the mass ratio.

Limiting case

Now we will consider what happens as the static compression gets large. We start with Eq. 5.11 for comparison. In this case the frequencies of the defect and the band edge both grow, as a result of larger static compressions, but everything else stays constant. In Eq. 5.11, the ratio f_d/f_r grows large and the added 1 in the first factor can be ignored. By rearranging we arrive at,

$$\left(-\frac{f_r^2}{f_d^2} \right) \frac{m_r}{m_0} = \left[\frac{m_s}{m_0} \left(1 \pm \sqrt{1 - \frac{f_c^2}{f_d^2}} \right) - 1 \right]. \quad (5.14)$$

The term on the left approaches zero and we are left with the relation for a simple mass defect.

$$\frac{m_0}{m_s} = \left(1 \pm \sqrt{1 - \frac{\omega_c^2}{\omega^2}} \right) \quad (5.15)$$

Therefore, in the case of extremely large compressions (and when the defect mass is smaller than the masses in the lattice, $m_0 < m_s$), the resonant defect acts as a simple mass defect, m_0 .

Control through design

By designing resonant defects with different geometries, we can tune several properties of the defect mode: the frequency of the defect mode (Fig. 5.8a), the rate at which the mode's profile changes with compression, the compression at which the mode becomes completely delocalized, and the mode's limiting profile at large compression forces (Fig. 5.8b). These properties can be adjusted through design by choosing the total mass, $m_0 + m_r$, resonating mass, m_r , and resonance frequency, f_r . Although somewhat counterintuitive, the frequency of defect modes with a smaller resonating mass are less affected by changes in compression of the lattice, as can be seen in Fig 5.8a. In addition, when the defect mass, m_0 , is less than the rest of the lattice, $m_0 < m_s$, the mode never becomes completely delocalized. Instead, as the compression is increased the mode profile approaches the shape of a simple mass defect mode with mass m_0 . The analytical section below illustrates how this design control manifests itself.

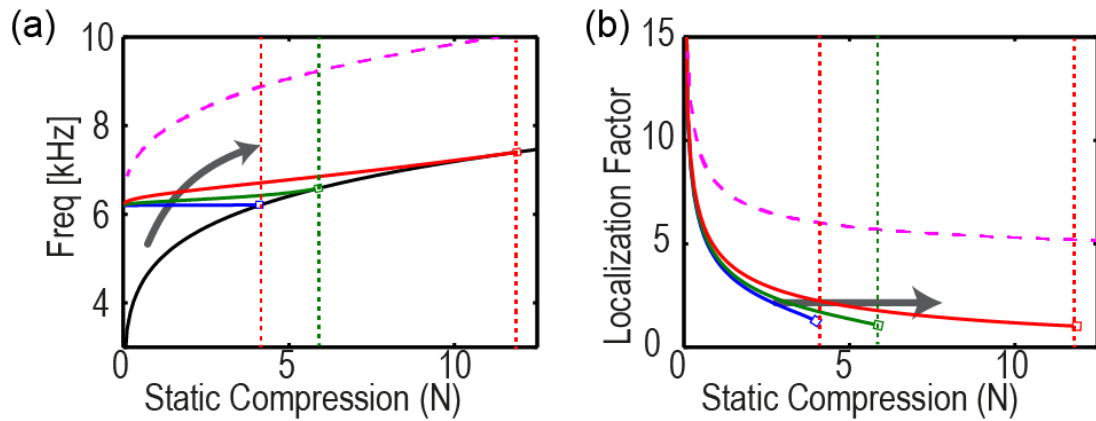


Figure 5.8: Tailoring the Resonator Design. (a) The effect of varying defect parameters on the mode frequency. The results for three resonant masses, m_r (solid lines) and one m_0 (dashed line). The arrow shows increasing m_r . (b) The localization of the defect mode for the same parameters shown in (a). For $m_0 < m_s$ (dashed line) the mode never delocalizes but asymptotically approaches the value of the localization for a mass defect of equivalent size, m_0 . The three vertical dashed lines indicate the compression at which the modes delocalizes when $m_0 < m_s$.

5.5 Conclusion

We have presented a method to actively control the localization of a defect mode in a nonlinear lattice of one and two dimensions. The results are easily extendable to three dimensions. The defect mode that results from a resonant defect has an additional degree of freedom that allows this tunability. This is the first time that a defect mode profile can be actively controlled and tuned without having to change the defect itself. In addition, since the same underlying principles of band tunability apply to a broad range of material systems, we anticipate that these results will impact current device and material applications.

5.6 Author contributions

The results from this chapter are from “Local to Extended Transitions of Resonant Defect modes”³⁷. Joseph Lydon and Marc Serra-Garcia developed the system concept and contributed

equally to the project. Joseph Lydon developed the numerical analysis and Marc Serra-Garcia developed the analytical study. Joseph Lydon and Marc Serra-Garcia performed the experimental work. Chiara Daraio contributed to the analysis. All authors contributed to the writing and editing of the section.

